Nuclear Physics B 375 (1992) 665–693
North-Holland

NUCLEAR
PHYSICS B

# Instabilities and interactions of global topological defects

Leandros Perivolaropoulos

*Division of Theoretical Astrophysics, MS-51, Harvard–Smithsonian Center for Astrophysics, 60 Garden Street, Cambridge, MA 02138, USA*
and
*Department of Physics, Brown University, Providence, RI 02912, USA*

Received 22 April 1991
(Revised 18 November 1991)
Accepted for publication 2 December 1991

The dynamics of global topological defects are investigated. The stability towards radial rescaling of global monopoles and vortices is verified and virial theorems connecting the potential and gradient energies are obtained. The validity of these theorems is demonstrated numerically. The angular monopole instability first discussed by Goldhaber is also examined. It is shown that even though his are correct, this instability manifests itself as motion of the monopole core rather than unwinding. The interactions of global defects are studied both analytically and numerically. An analytical derivation of their interaction potential is followed by numerical simulation verifying the predicted potential. Using boosted field configurations we demonstrate the existence of critical velocities for defect scattering and annihilation.

## 1. Introduction

Topological defects are predicted by many particle physics models to form during phase transitions in the early universe. Such phase transitions are caused by spontaneously broken symmetries leading to a manifold of degenerate vacua with nontrivial topology. Several types of defects may form depending on the topology of the vacuum manifold: domain walls, vortices [1], monopoles or textures. If the broken symmetry is gauged, the emerging defects have finite energy and their mass is concentrated in a small core. On the other hand, the breaking of a global symmetry may lead to defects with diverging mass, due to the long range of the Nambu–Goldstone field. Such divergences, even though unphysical for isolated defects, are easily realized in a cosmological setup. The horizon scale, which is the typical distance between global defects, provides a natural cutoff for their energy density.

The vast majority of the literature had until recently focused on gauged defects. There are two basic reasons for this. First, most grand unified theories predict the

existence of local defects. In order to include broken global symmetries one would have to extend the grand unified theory models. Thus, even though broken global symmetries are not inconsistent with the well known models, there is less theoretical motivation to consider global defects. Second, the study of their formation and evolution on large scales is more complicated than the corresponding study for their gauged counterparts. This is mainly due to the long-range Nambu–Goldstone field which makes the use of simplified actions (e.g. the Nambu action for vortices) inappropriate for describing their evolution.

Recently however, the study of global defects has attracted significant attention. This is due to several reasons. First, their long range interactions rapidly increase their correlation length to the maximum allowed by causality: the horizon scale. Thus global defects are more efficient in forming very-large-scale structures in the universe than their gauged counterparts. This interaction has an additional important effect: it introduces an efficient decay mechanism which prevents them from dominating the energy density of the universe. For example, global monopoles do not contradict standard cosmology [8,9,12] in contrast to their local counterparts. Finally, global defects are interesting toy models on which the field theory of the more complicated gauged defects may be studied.

In order to understand the cosmological effects of global defects like monopoles and vortices, it is important to study both their gravitational field [7,8], and their dynamics and interactions [3]. Attempts to study the dynamics of vortices and monopoles have led to various controversial points. Many open issues remain: Is the Nambu action appropriate for describing the evolution of vortices? Are global monopoles stable? What is the detailed form of the interaction between global monopoles?

This paper is an attempt to shed some light to the questions involving the dynamics of global monopoles. The dynamics of vortices are also studied, in order to make contact with previous studies.

The monopole stability towards radial rescaling and angular perturbations is investigated in sect. [2]. If Derrick's theorem was valid for global monopoles they would be unstable towards radial rescaling of the field configuration. However their linearly divergent mass makes Derrick's theorem inapplicable. A careful study shows that the global monopole field configuration is in fact stable towards radial rescaling. A virial theorem connecting the gradient with the potential energy is also derived and its validity is demonstrated by numerically solving the field equations. Similar results are obtained for vortices. Sect. 3 focuses on the effect of angular perturbations. It is demonstrated that for an isolated monopole with an imposed cutoff, it is energetically favorable for angular perturbations on a fixed spherical shell to grow. However, it is shown that this growth of perturbations does not correspond to monopole unwinding; it corresponds to monopole motion. The obtained semi-analytical results are demonstrated by numerical simulations. The interactions of global monopoles are studied in sect. 4. The detailed form of the

interaction potential is obtained and its dominant part at large distances is verified by a numerical simulation. The scattering of two highly-relativistic global monopoles produces a ring-shaped vortex-like configuration which subsequently expands at right angles with respect to the line of incidence. It is also demonstrated that the scattering of a monopole–antimonopole pair with velocities larger than a critical one (about equal to $0.8c$) with respect to the center of mass, does not lead to annihilation. Similar results are obtained for the case of vortices. Finally in sect. 5 conclusions are drawn with regard to possible implications of our results for the cosmological effects and field theoretical properties of global monopoles.

In the following analysis we normalize fields, masses and space coordinates to dimensionless quantities using the scale of symmetry breaking that gives rise to the investigated topological defects.

## 2. Radial rescaling: Virial theorems

The simplest lagrangian density that describes the evolution of global monopoles is of the form

$$\mathscr{L} = \tfrac{1}{2}\partial_\mu \boldsymbol{\Phi} \cdot \partial^\mu \boldsymbol{\Phi} - \tfrac{1}{4}\lambda(\boldsymbol{\Phi} \cdot \boldsymbol{\Phi} - 1)^2, \tag{2.1}$$

where $\boldsymbol{\Phi}$ is a Higgs field with an O(3) symmetry. This lagrangian gives rise to a global symmetry breaking $O(3) \to O(2)$. The vacuum manifold is $S^2$ implying the existence of spherically symmetric, topologically non-trivial solutions. Such monopole solutions are described by the ansatz

$$\boldsymbol{\Phi} = f(r)\frac{\boldsymbol{r}}{r}, \tag{2.2}$$

with boundary conditions $f(r \to 0) \to 0$ and $f(r \to \infty) \to 1$. It is easy to show that the boundary conditions $f(r \to R) \to 1$ would only modify $f(r)$ by terms of $O(R^{-2})$. This is a three-dimensional scalar field configuration. Derrick's theorem states that any finite-energy scalar field configuration in $d \geqslant 3$ ($d$ is the number of spatial dimensions) is unstable towards shrinking and collapse. Since the energy of the global monopole is linearly divergent, Derrick's theorem is not applicable in this case. However this does not automatically imply that global monopoles are stable towards radial rescaling. To address this issue we must check whether the energy of the monopole corresponding to a rescaled field $f(\alpha r)$ has a minimum with respect to the rescaling parameter $\alpha$. The energy resulting from such a rescaling is of the form

$$E_\alpha^{\mathrm{m}} = \frac{4\pi}{\sqrt{\lambda}}\alpha^{-1}\left[I_1^{\mathrm{m}}(\alpha R) + I_2^{\mathrm{m}}(\alpha R) + \tfrac{1}{4}\alpha^{-2} I_3^{\mathrm{m}}(\alpha R)\right], \tag{2.3}$$

with

$$I_1^{\mathrm{m}}(\alpha R) = \int_0^{\alpha R} \mathrm{d}r\, r^2 \frac{f'^2(r)}{2},$$

$$I_2^{\mathrm{m}}(\alpha R) = \int_0^{\alpha R} \mathrm{d}r\, f^2(r),$$

$$I_3^{\mathrm{m}}(\alpha R) = \int_0^{\alpha R} \mathrm{d}r\, r^2 \left(f^2(r) - 1\right)^2, \tag{2.4}$$

where $R$ is a cutoff naturally imposed in a cosmological setup and $r$ has been rescaled by the scale of symmetry breaking $\eta$ to the dimensionless form $\sqrt{\lambda}\,\eta r$. The superscript m stands for "monopole". Stability implies that the conditions

$$\left.\frac{\partial E_\alpha}{\partial \alpha}\right|_{\alpha=1} = 0,$$

$$\left.\frac{\partial^2 E_\alpha}{\partial \alpha^2}\right|_{\alpha=1} \geqslant 0, \tag{2.5}$$

are satisfied. Using (2.3) in (2.5) we obtain

$$I_1^{\mathrm{m}}(R) + I_2^{\mathrm{m}}(R) + \tfrac{3}{4} I_3^{\mathrm{m}}(R) = R, \tag{2.6a}$$

$$I_1^{\mathrm{m}}(R) + I_2^{\mathrm{m}}(R) + \tfrac{9}{4} I_3^{\mathrm{m}}(R) \geqslant 0, \tag{2.6b}$$

where we have ignored terms of $\mathcal{O}(R^{-1})$ but have included all terms of $\mathcal{O}(1)$. Thus, the virial condition (2.6a) which connects the monopole gradient and potential energies is exact to $\mathcal{O}(1)$.

Since $I_1^{\mathrm{m}}$, $I_2^{\mathrm{m}}$, $I_3^{\mathrm{m}} \geqslant 0$ condition (2.6b) is obviously satisfied. Due to the divergent term, both sides of (2.6a) are positive. Therefore it may have a solution which must be identical to the solution of the monopole equations of motion resulting from variation of the lagrangian (2.1). It is straightforward to solve these equations of motion numerically, using the ansatz (2.2). The solution $f(r)$ is linear for small $r$ as may be verified analytically. Its slope at the origin is 0.50 while the corresponding result for vortices [3] is 0.58. Using this solution we may calculate the quantities $I_1^{\mathrm{m}}$, $I_2^{\mathrm{m}}$ and $I_3^{\mathrm{m}}$ corresponding to the radial gradient, angular gradient and potential energies respectively. In fig. 1 we plot the left-hand side of eq. (2.6a) versus the cutoff $R$. The result is a straight line with slope $1.03 \pm 0.05$ in good agreement with the slope of 1.0 predicted by eq. (2.6a). Thus not only has the radial stability of global monopoles been verified but also we have derived a virial theorem connecting the gradient and potential energies to the cutoff scale.

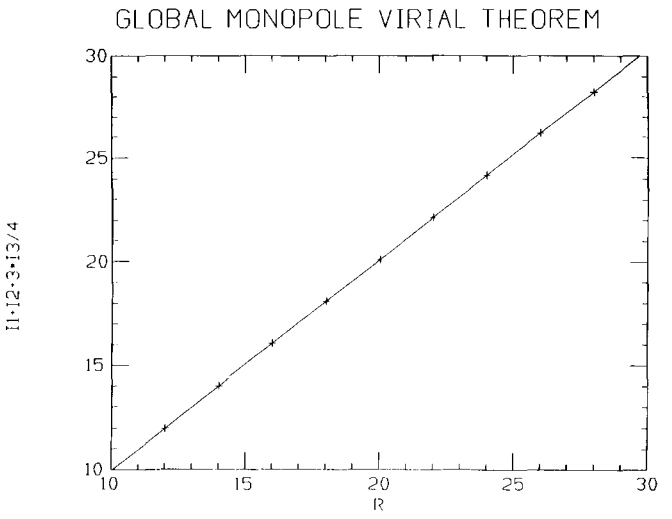


Fig. 1. Numerical verification of the virial theorem for global monopoles. Predicted slope: 1.0. Numerically obtained slope: $1.03 \pm 0.05$.

The physical reason for the radial stability of the global monopoles is the balance between the potential energy term $I_3^{\mathrm{m}}(R)$ which favors shrinking and collapse of the field, and the diverging angular gradient term $I_2^{\mathrm{m}}(R)$ which favors expansion of the monopole configuration.

It is straightforward to extend the above analysis to the case of vortices. In this case the field of the lagrangian density (2.1) is a complex singlet while the symmetry breaking is $\mathrm{U}(1) \to \mathrm{I}$, giving rise to vertices since the vacuum manifold is now $\mathrm{S}^1$. The vortex ansatz has the cylindrically symmetric form

$$\boldsymbol{\Phi}(\boldsymbol{\rho}) = f(\rho)\frac{\boldsymbol{\rho}}{\rho}, \tag{2.7}$$

where $\boldsymbol{\Phi}$ is written as a two component vector on the complex plane. The rescaled energy per unit length of the vortex is

$$\frac{\mathrm{d}E_\alpha^{\mathrm{v}}}{\mathrm{d}l} = \pi\left[I_1^{\mathrm{v}}(\alpha R) + I_2^{\mathrm{v}}(\alpha R) + \tfrac{1}{2}\alpha^{-2} I_3^{\mathrm{v}}(\alpha R)\right], \tag{2.8}$$

with

$$I_1^{\mathrm{v}}(\alpha R) = \int_0^{\alpha R} \mathrm{d}\rho\, \rho f'^2(\rho),$$

$$I_2^{\mathrm{v}}(\alpha R) = \int_0^{\alpha R} \frac{\mathrm{d}\rho}{\rho} f^2(\rho),$$

$$I_3^{\mathrm{v}}(\alpha R) = \int_0^{\alpha R} \mathrm{d}\rho\, \rho\left(f^2(\rho) - 1\right)^2, \tag{2.9}$$

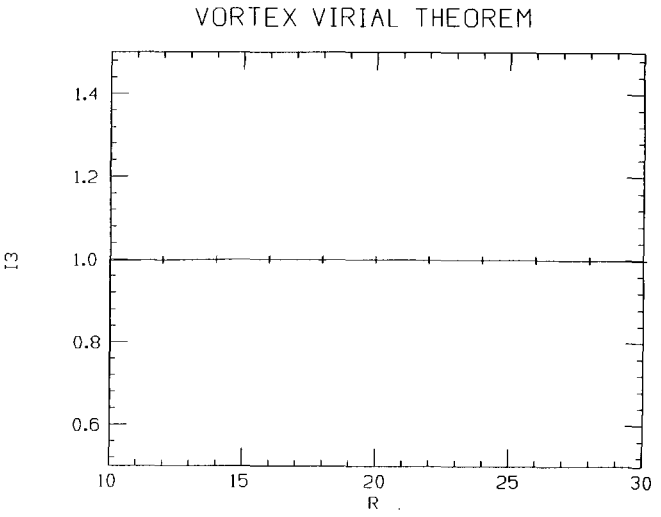


Fig. 2. Numerical verification of the virial theorem for vortices. Predicted value for potential energy $I_3$: 1.0. Numerically obtained value: $1.0 \pm 0.02$.

where the superscript v stands for "vortex". Minimizing with respect to $\alpha$ (conditions (2.5)) leads to the virial theorem

$$I_3^{\mathrm{v}}(R) = 1, \tag{2.10a}$$

$$I_3^{\mathrm{v}}(R) \geqslant \tfrac{1}{3}. \tag{2.10b}$$

Notice that (2.10a) is exact for $R \to \infty$. Obviously (2.10b) is always satisfied given (2.10a). It is straightforward to solve the equations of motion for $f(\rho)$ numerically. The slope of $f(\rho)$ at small $\rho$ is 0.58 in agreement with ref. [3]. In order to check the virial condition (2.10a) we plot $I_3^{\mathrm{v}}(R)$ versus the cutoff $R$ in fig. 2. The numerical results clearly verify the analytical prediction (2.10a).

Thus the radial stability of global vortices has also been checked, their potential energy has been analytically calculated and the result numerically verified.

## 3. Angular instabilities of global monopoles

The stability of global monopoles towards angular perturbations clearly plays a crucial role on the evolution of the field configuration after the phase transition. This issue has recently become the source of significant controversy. In ref. [2] Goldhaber claimed that there is an energy gradient favoring the unwinding of an isolated but finite-size global monopole, after an initial angular perturbation. On the other hand the claim of ref. [4] was that in fact such an energy gradient does not exist and only unrealistically large thermal fluctuations could lead to monopole

unwinding and decay. This section is an attempt to shed some light on this controversy. Using semi-analytical methods it will be shown that the claims of ref. [2] are valid. There are energy gradients that favor the amplification of an initial angular perturbation on any spherical shell surrounding a global monopole. However, it will be shown that the smaller the spherical shell the larger these gradients are. Thus the unwinding will start from the inner shells and then proceed to the outer ones. Such an evolution can not be distinguished from the motion of the monopole core in the direction of the reduced field magnitude. This evolution is indeed seen in our numerical simulation of an angularly perturbed global monopole.

In order to study the effect of angular perturbations it is convenient to use an ansatz which describes the monopole configuration on a fixed spherical shell of radius $r$ much larger than the monopole core. This ansatz is of the form

$$\Phi_1 = f(\theta)\ \sin\bar{\theta}(\theta)\ \cos\varphi,$$

$$\Phi_2 = f(\theta)\ \sin\bar{\theta}(\theta)\ \sin\varphi,$$

$$\Phi_3 = f(\theta)\ \cos\bar{\theta}(\theta). \tag{3.1}$$

It is straightforward to use this ansatz to calculate the energy of the monopole on the fixed spherical shell. The change of variables $\theta \to y = \ln(\tan(\theta/2))$ significantly simplifies the form of the final expression. The result is

$$E = \tfrac{1}{2}\int_r \mathrm{d}y\ \mathrm{d}\varphi\left[f'^2 + \frac{\alpha}{\cosh^2 y}\left(f^2-1\right)^2 + f^2\left(\bar{\theta}'^2 + \sin^2\bar{\theta}\right)\right], \tag{3.2}$$

where $\alpha = \frac{1}{2}\lambda\eta^2 r^2$ and the prime denotes derivative with respect to the new angular variable $y$. This is the same expression obtained in ref. [2] (up to some typos which we have corrected and ignoring the time dependence of $\bar{\theta}$). The crucial observation made there was that the part of (3.2) that depends on $\bar{\theta}$ is exactly the energy of a sine–Gordon soliton. Therefore we may substitute $\bar{\theta}$ in (3.2) by the sine–Gordon solution which minimizes this part of the energy functional. This argument however, assumes that $f'$ is negligible. Indeed, it is easily verified that the equations of motion for $f$ and $\bar{\theta}$ accept a sine–Gordon solution for $\bar{\theta}$ only if $f'(y)$ is zero. Such an assumption is valid for a monopole solution but not for an unwinding configuration. However, it may be shown that neglecting $f'(y)$ does not change the final result. Therefore, here we will neglect $f'(y)$ to simplify the analysis.

The sine–Gordon solution to be substituted in eq. (3.2) is

$$\bar{\theta}(y) = 2\ \tan^{-1}\mathrm{e}^{(y-y_0)}, \tag{3.3}$$

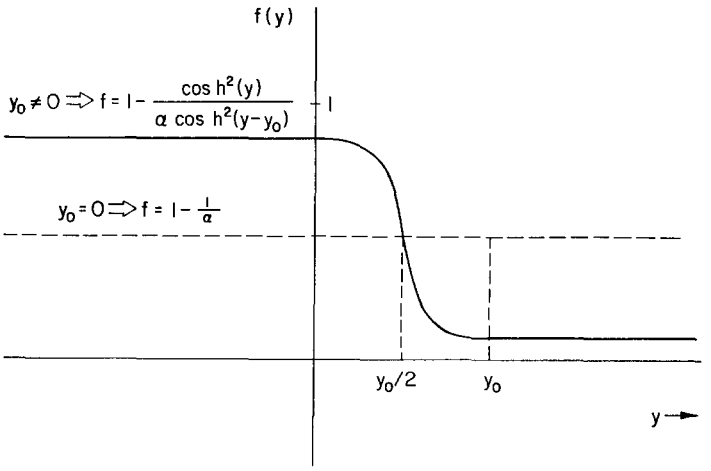


Fig. 3. The angular dependence of the field $f(y)$ that minimizes the potential energy. Notice the angular dependence that is introduced for $y_0 \neq 0$.

where $y_0$ is an arbitrary constant resulting from translational invariance. Using (3.3) in eq. (3.2) we obtain the potential energy density

$$U(f) = \frac{f^2}{\cosh^2(y - y_0)} + \frac{\alpha(f^2-1)^2}{2\cosh^2(y)}. \tag{3.4}$$

The function $f_{\min}(y)$ that minimizes the above potential energy density is

$$f^2_{\min}(y) = 0, \qquad \alpha \leqslant \frac{\cosh^2 y}{\cosh^2(y - y_0)}$$

$$f^2_{\min}(y) = 1 - \frac{\cosh^2 y}{\alpha \cosh^2(y - y_0)}, \quad \alpha \geqslant \frac{\cosh^2 y}{\cosh^2(y - y_0)}. \tag{3.5}$$

This function is shown in fig. 3 for $y_0 = 0$ and $y_0 \neq 0$.

For $y_0 = 0$ the field is spherically symmetric and is identified with the monopole configuration (notice that $f \simeq 1 - (1/2\alpha)$ gives the correct asymptotic radial power law behavior for monopoles). However for $y_0 \neq 0$ the field varies with the polar angle and for $y_0$ larger than a critical value determined by $\alpha = \cosh^2 y/(\cosh^2(y - y_0))$ it goes to zero along the south pole $\theta = \pi$ $(y \to +\infty)$. In this case the configuration becomes trivial and nothing can prevent the monopole from unwinding on the particular shell determined by $\alpha$.

The question that should be addressed is the following: Given an initial topologically non-trivial spherically symmetric configuration $(y_0 = 0)$, on a fixed

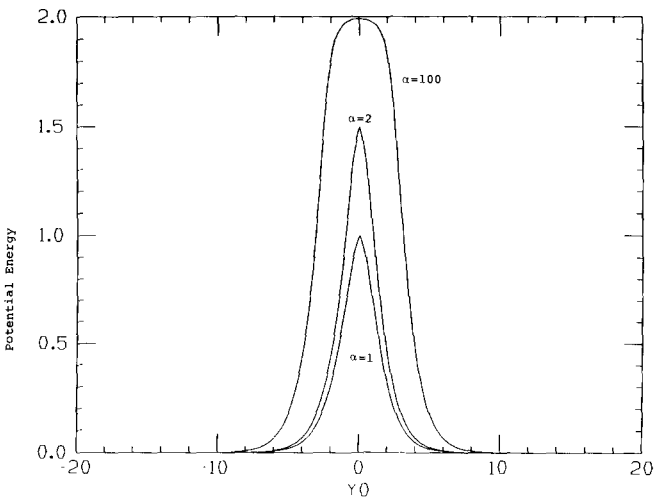


Fig. 4. The total potential energy for $\alpha = 1$, $\alpha = 2$ and $\alpha = 100$ obtained by using the $f(y)$ of fig. 3 in the integral for the potential energy. The energy maximum increase with $\alpha$. Notice that configurations with large $|y_0|$ (i.e. high angular distortion) are energetically favorable for all values of $\alpha$.

shell of radius $r$ are there energy gradients that will favor a configuration with $y_0 \to +\infty(-\infty)$, leading the global monopole to unwind from the south (north) pole? To address this question we have calculated the total potential energy: $V_{\text{tot}}(y_0) = \int_{-\infty}^{+\infty} \mathrm{d}y\ U(f_{\min}(y,\ y_0))$ for a range of values of $y_0$. The results are plotted in fig. 4 for $\alpha = 1$, $\alpha = 2$ and $\alpha = 100$. Notice that even though in all cases the spherically symmetric solution $y_0 = 0$ is a stationary point of the energy functional, it is also an unstable point. Energy gradients tend to amplify any initial angular perturbation. This result remains valid even if we include the gradient term $f'(y)$ in the energy functional.

The important thing to observe in fig. 4 is that the energy gradients that favor unwinding decrease as the shell radius increases. Therefore it is the inner shells that develop a zero along the south pole and unwind first. Clearly, such an evolution is identical to motion of the monopole core in the direction $\theta = \pi$ or $\theta = -\pi$ depending on the initial perturbation.

It is interesting to check the above semi-analytical results using a numerical simulation. In order to study the way the monopole instability proceeds we can not use the $\sigma$-model approximation used in ref. [9] since this would artificially exclude the possibility of reduced magnitude of the field. Therefore, we have solved the full equations of motion obtained from the lagrangian (2.1) on a $48^3$ lattice, using a leapfrog algorithm. The boundary conditions used were reflective (the first derivative of the field was taken to be zero at the boundaries) while the lattice spacing and timestep were $\mathrm{d}x = 0.5$ and $\mathrm{d}t = 0.1$ respectively. The Courant stability criterion was therefore satisfied. The fact that the timestep is smaller than the Courant number $\mathrm{d}t \simeq 0.3$ introduces a small numerical viscosity implying a spurious de-

crease of the wave mode amplitude on large timescales. On the timescale of our simulation however there was no significant effect from numerical viscosity as can be verified from the energy conservation tests that we performed. The equations of motion solved during the simulation are

$$\partial^2 \Phi = \Phi(\Phi^2 - 1). \tag{3.6}$$

The energy conservation was better than 3% for all runs (up to 1000 timesteps). We first used initial conditions corresponding to an unperturbed monopole: $\Phi = r/r$. The field configuration kept oscillating without violating spherical sym-

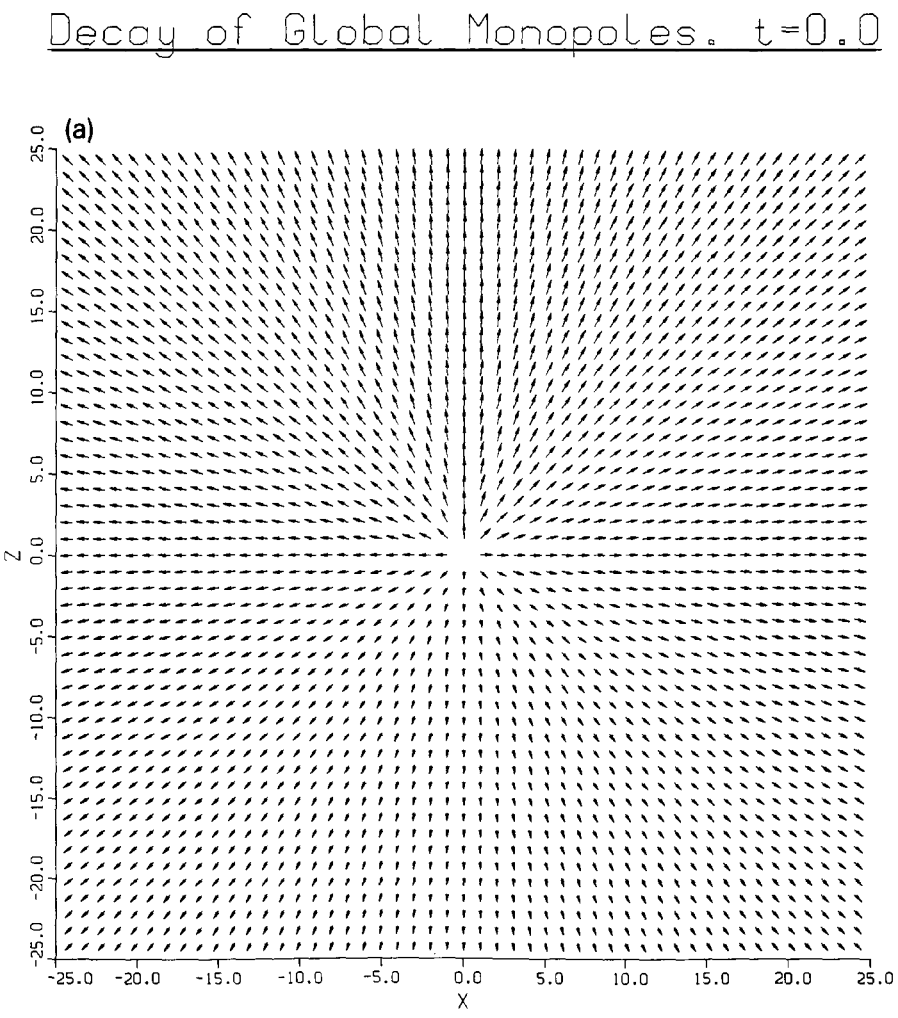


Fig. 5. The evolution of an angularly perturbed global monopole. The field on the $x-z$ plane is plotted. (a) $t = 0$; (b) $t = 20.0$. The field initially tends to zero along the south pole ($\theta = \pi$). The inner shells unwind first resulting to a monopole motion and decay at the boundary.

metry. These oscillations are the result of competing angular gradient (favoring expansion) and potential (favoring collapse) energies as explained in sect. 2. We then perturbed the monopole configuration by decreasing the field magnitude along the south pole ($\theta = \pi$). This was achieved by the initial conditions: $\Phi = (r/r)[(2\pi - \theta)/2\pi]$. The evolution of this perturbed configuration is shown in fig. 5. As predicted, the initial perturbation gets amplified, the field tends to zero for $\theta = \pi$. However, it is the inner shells that unwind first, resulting to motion of the monopole core in the direction of the perturbation.

The physical reason for this instability is the competition between the angular gradient energy, which favors reduced field magnitude and subsequent unwinding

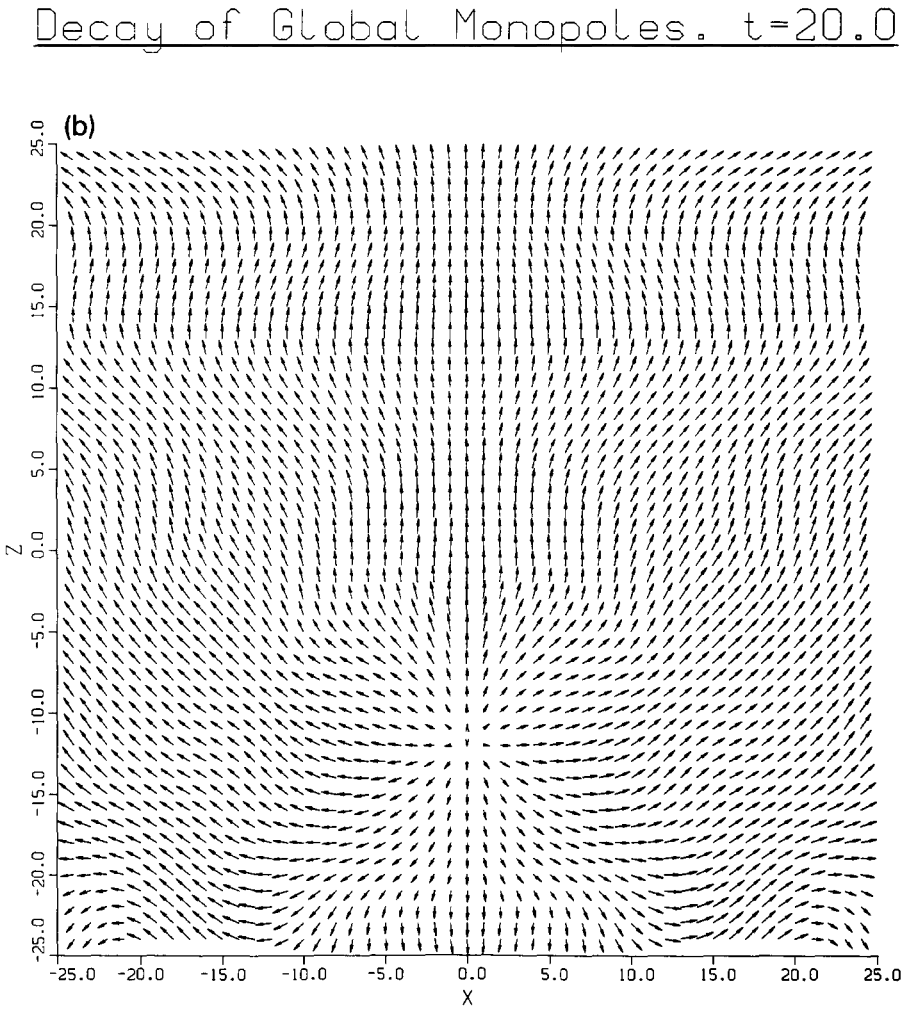


Fig. 5b.

and the potential energy, which tends to confine the field in the vacuum manifold and thus prevent the unwinding. The angular energy density is larger for the inner shells and therefore the unwinding starts from them. We also performed a similar simulation for an angularly perturbed straight vortex, with similar results. The vortex core indeed moved in the direction of reduced field magnitude.

The above analysis has focused on an isolated perturbed global monopole with no velocity. In a realistic situation however, monopole interactions will introduce non-zero velocities and specific types of boundary conditions. It is important to understand what is the effect of the angular perturbation on a finite energy system

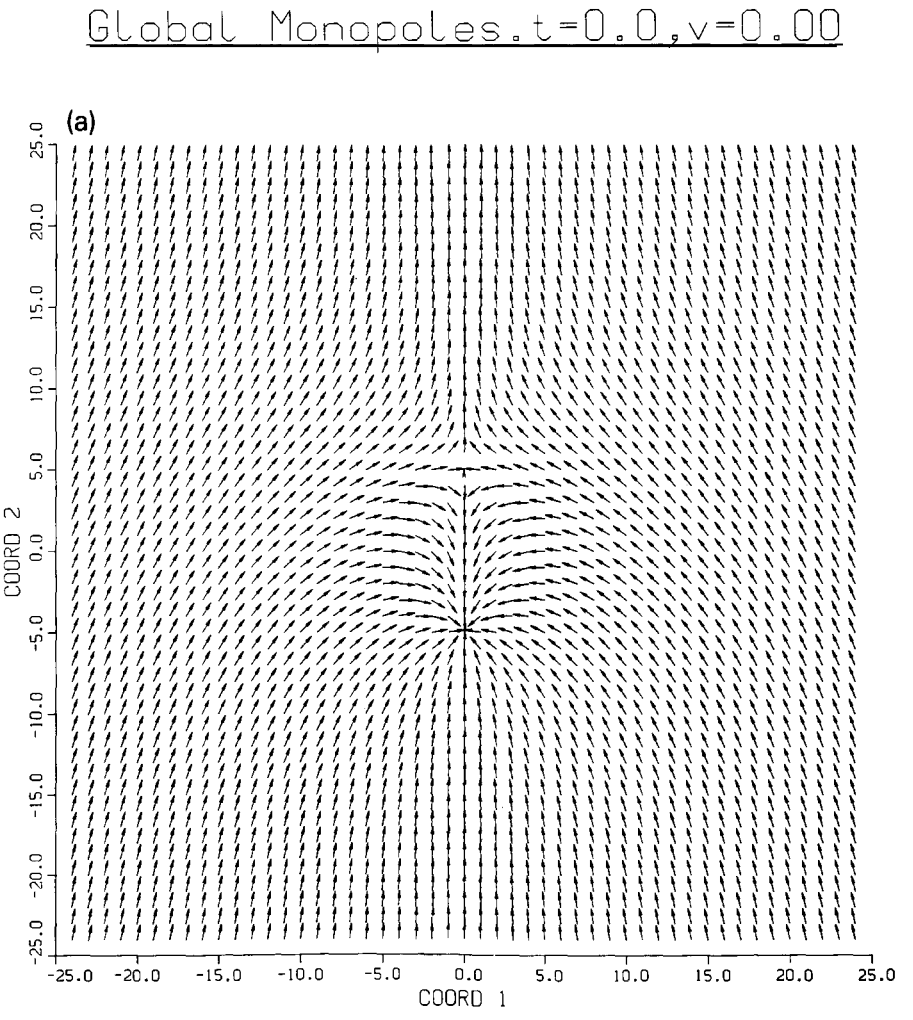


Fig. 6. The evolution of monopole–antimonopole pair. (a) $t = 0$, $v = 0$; (b) $t = 7.5$. The pair attracts and annihilates into radiation.

of monopoles. We have evolved the axially symmetric monopole–antimonopole system shown in fig. 6a. As is shown in sect. 4 there is a constant attractive force equal to $4\pi^2$ in such a monopole–antimonopole system. As predicted the monopole configurations are not unwinding uniformly. Instead the unwinding proceeds from the inner shells to the outer. Unless the monopole cores are held fixed during the evolution, this behavior manifests itself as acceleration of the monopole cores towards the origin where annihilation into radiation takes place (fig. 6b).

To summarize, even though the results of this section agree with the arguments of ref. 2, it is shown that these arguments should not be interpreted as monopole

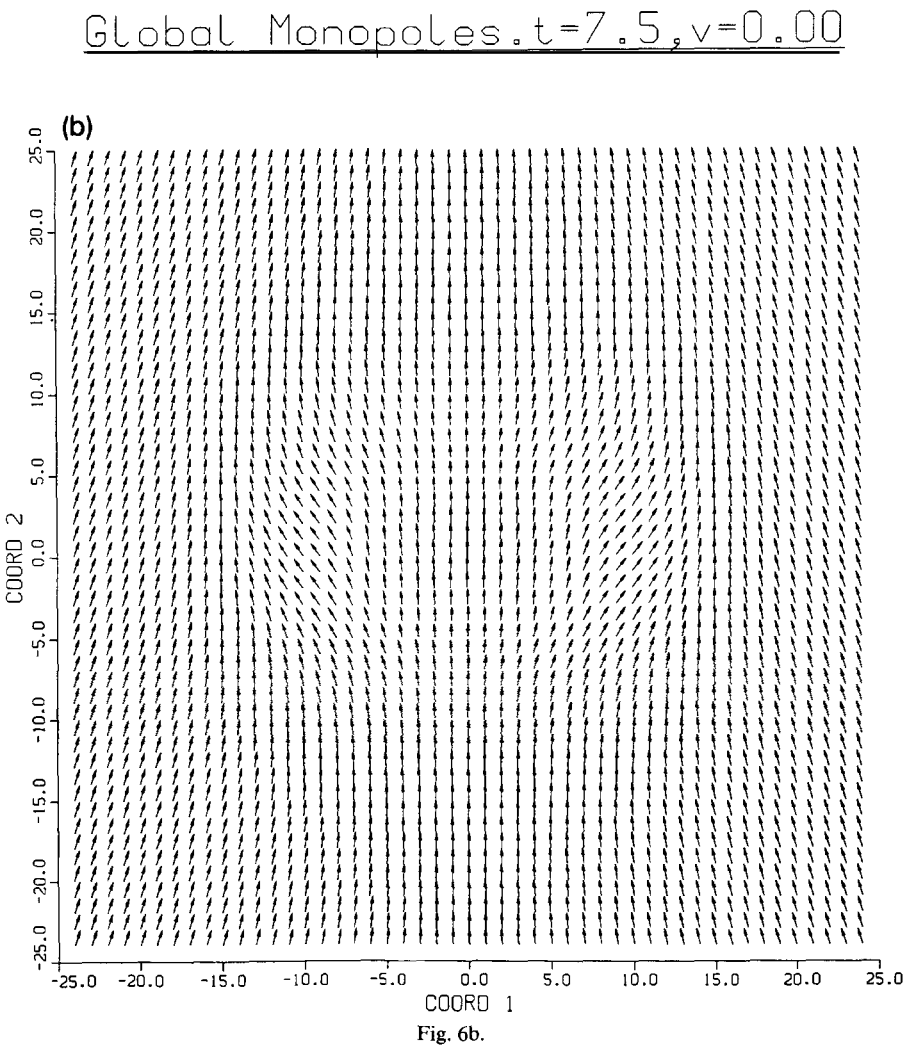


Fig. 6b.

collapse but as motion of the monopole towards the region of the reduced field magnitude. This conclusion is consistent with other recent studies [4,5].

## 4. Interactions of global defects

The study of the interaction of global defects is important in order to understand their general evolution properties. In this section we focus on the interactions of a/vortices and b/global monopoles, using both analytical methods and numerical simulations. In all cases, we will consider a pair of global defects placed

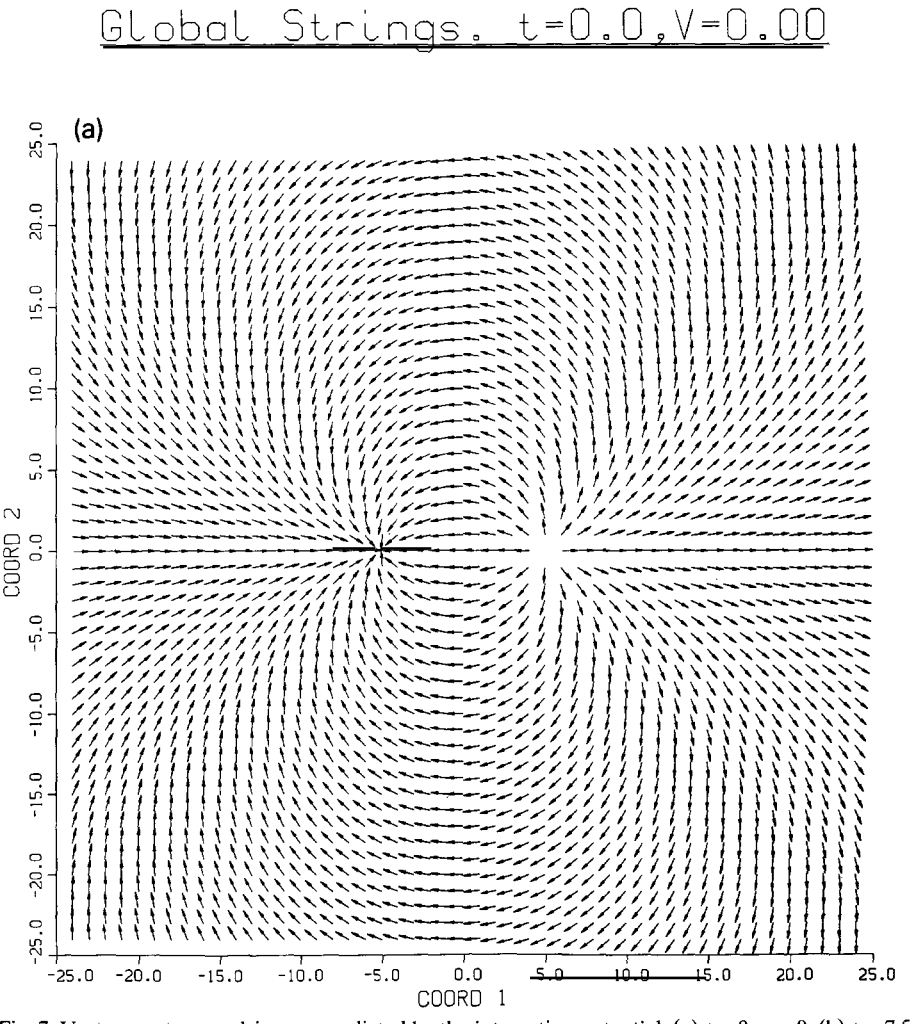


Fig. 7. Vortex–vortex repulsion, as predicted by the interaction potential. (a) $t = 0$, $v = 0$; (b) $t = 7.5$.

at a distance $2a$ from each other, much larger than their core radius. The interaction potential will be derived in each case and it will be verified by a numerical simulation of evolution. Boosted configurations will also be considered in order to study the existence of critical velocities.

Consider a pair of vortices with core centers at $\boldsymbol{\rho}_1$ and $\boldsymbol{\rho}_2$. The field configuration away from the vortex cores is well approximated by [3]

$$\Phi^{\pm}_{\text{tot}}(\boldsymbol{\rho}) = e^{i(\theta_1 \pm \theta_2)}, \tag{4.1}$$

where $\theta_1$ and $\theta_2$ are the azimuthal angles with respect to the two centers and the

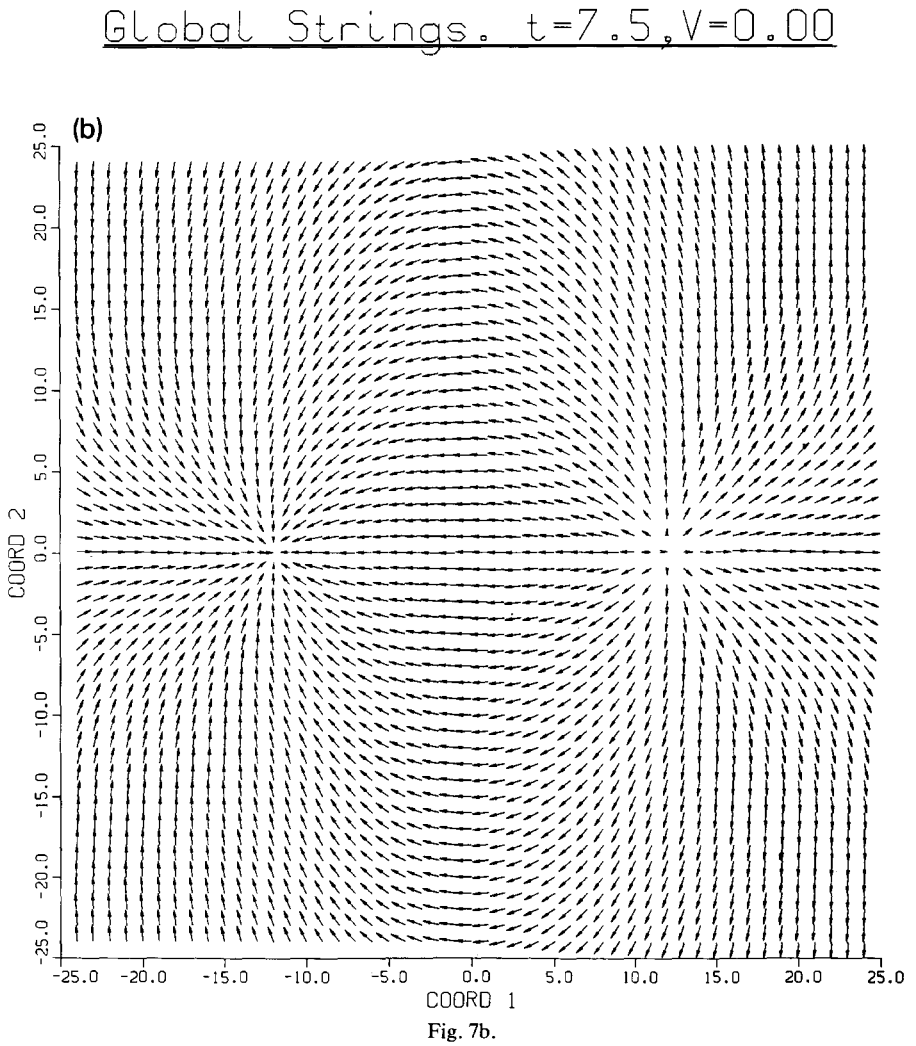


Fig. 7b.

upper (lower) sign refers to a vortex–vortex (vortex–antivortex) pair. This ansatz was introduced in ref. [3] and was motivated by that of Abrikosov [10] for two gauged strings. It clearly gives the right topological charge for each of the vortices and smoothly interpolates between them. It is straightforward to obtain the interaction energy density between the two vortices by subtracting the sum of the individual vortex energies from the combined configuration energy. Thus, ignoring the deformation of the cores due to the interaction, we have

$$\varepsilon_{\text{int}}^{\pm} = \tfrac{1}{2}\left[\left(\nabla\Phi_{\text{tot}}^{\pm}\right)^2 - \left(\nabla\Phi_1\right)^2 - \left(\nabla\Phi_2^{\pm}\right)^2\right], \tag{4.2}$$

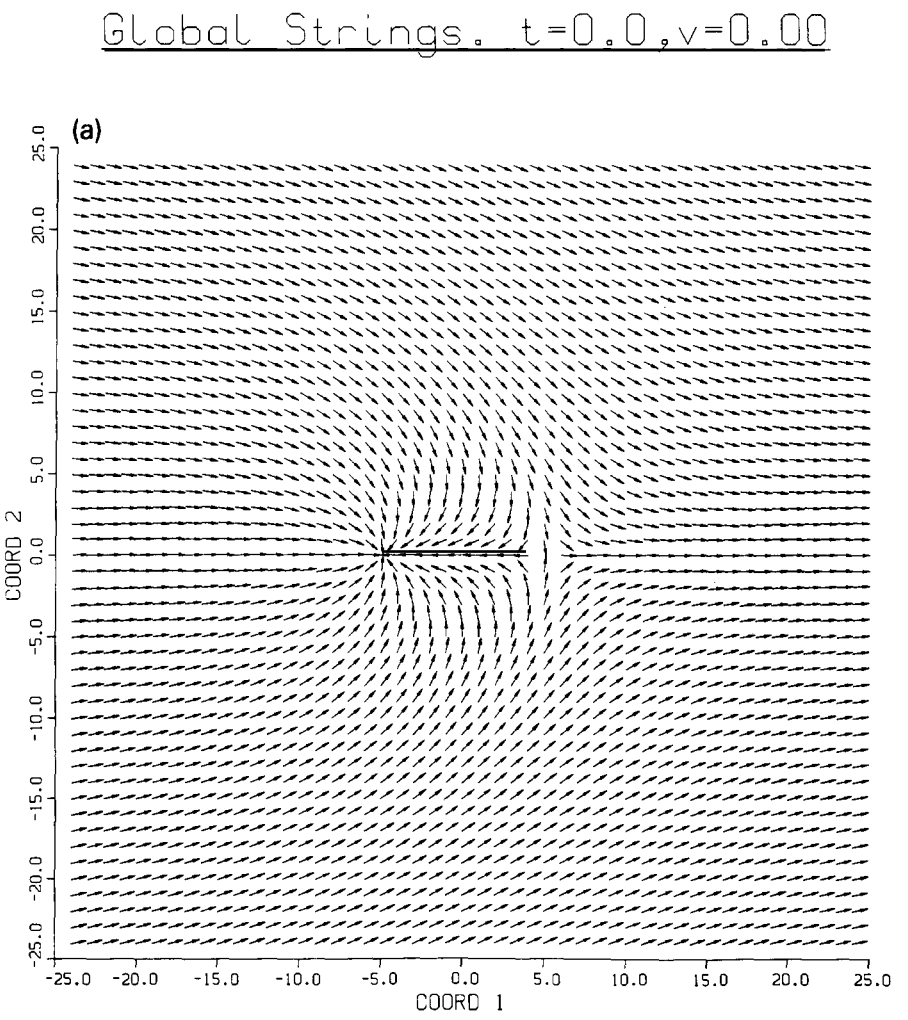


Fig. 8. Vortex–antivortex attraction and annihilation. (a) $t = 0$, $v = 0$; (b) $t = 7.5$. Notice the radiation propagating at right angles with respect to the line of incidence.

where $\Phi_1 = e^{i\theta_1}$ and $\Phi_2^{\pm} = e^{\pm i\theta_1}$. The resulting energy density is

$$\varepsilon_{\text{int}}^{\pm} = \pm \frac{\rho^2 - a^2}{(\rho^2 + a^2)^2}, \tag{4.3}$$

where $a$ is half the intervortex distance and $\rho$ is measured from the center between the two vortices. Notice that the interaction energy density is cylindrically symmetric even though the field configuration is not.

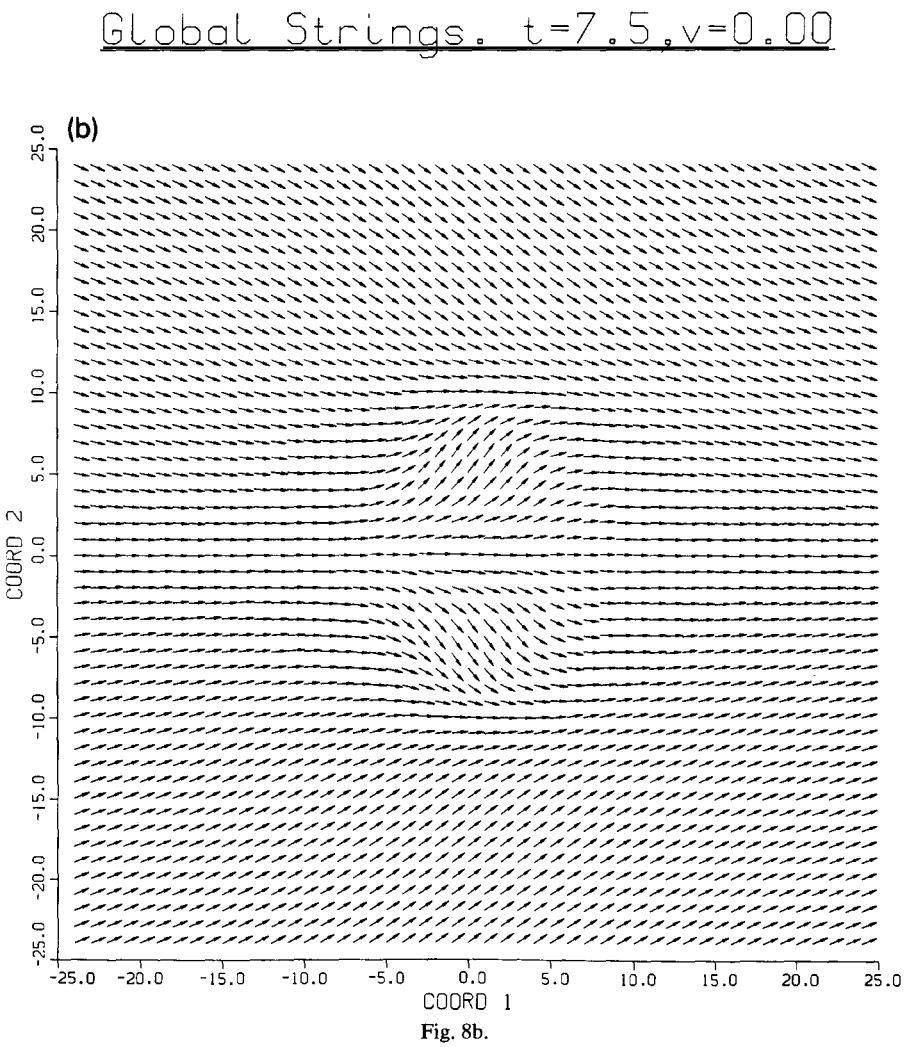


Fig. 8b.

The interaction potential is obtained by integrating (4.2) up to a cutoff $L$. The result is

$$E_{\rm int}^{\pm} = 2\pi \int_0^L d\rho\ \rho \varepsilon_{\rm int}^{\pm}(\rho) = \pm 2\pi \left( \frac{\log(L^2 + a^2)}{2} + \frac{a^2}{L^2 \mp a^2} - 1 - \log(a) \right)$$

$$\simeq \mp 2\pi (\log(a) - \log(L)), \tag{4.4}$$

where the assumption $L \gg a \gg 1$ was used. The corresponding force is

$$F_{\rm int}^{\pm} = -\frac{\partial E^{\pm}}{\partial a} \simeq \pm \frac{2\pi}{a}, \tag{4.5}$$

giving repulsion (attraction) for the vortex–vortex (vortex–antivortex) system. The result for the interaction force is in agreement with ref. [3] even though a different method was used there.

In order to verify the derived interaction potential we have performed a numerical simulation evolving the initial conditions (4.1). The code described in sect. 3 was used, with appropriate modifications to account for the substitution of global monopoles by vortices. In particular eqs. (3.7) were solved with $\Phi$ a two component field. The initial separation between the two vortices was five core-sizes.

The repulsion in a vortex–vortex configuration is demonstrated in fig. 7, while in fig. 8 the attraction and annihilation into radiation of a vortex–antivortex pair is shown.

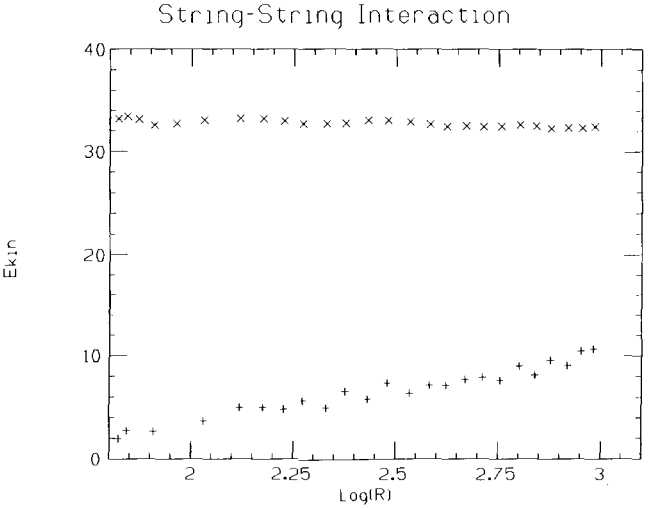


Fig. 9. The kinetic energy per unit length of a vortex–vortex configuration during evolution, as a function of the log of the vortex separation $R$ (+ symbol). The points are on a straight line to a good approximation. The slope is $7.4 \pm 1.0$ consistent with the predicted value $2\pi$. The conserved total energy is also plotted (× symbol).

The precise form of the interaction potential (4.3) may be checked by plotting the kinetic energy $E_{\text{kin}} = \frac{1}{2}\dot{\Phi}^2$ versus the log of the vortex separation $R = 2a$. Energy conservation implies that $E_{\text{int}} = \text{const.} - E_{\text{kin}}$ and therefore, by (4.4), the slope of $E_{\text{kin}}(\log(R))$ for a vortex–vortex pair should be positive and equal to $2\pi$. In fig. 9 we plot $E_{\text{kin}}$ versus $\log(R)$ (+ symbol in plot) as well as the conserved total energy (× symbol in plot). The function $E_{\text{kin}}$ $(\log(R))$ is indeed a straight line to a good approximation with slope $7.4 \pm 1.0$ which is consistent with the analytically predicted value $2\pi$.

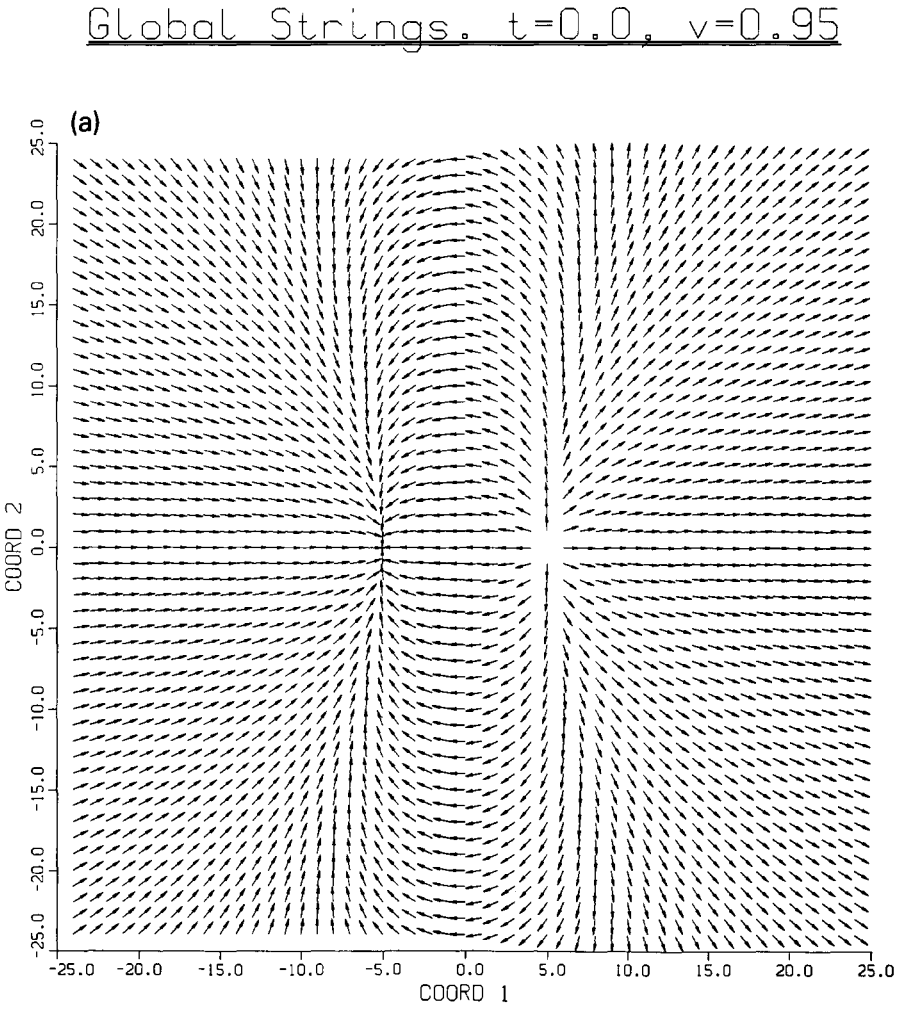


Fig. 10. Vortex–vortex scattering. (a) $t = 0$, $v = 0.95c$; (b) $t = 7.5$. The initial velocities in the center of mass frame necessary to overcome the repulsive interaction were $0.95c$.

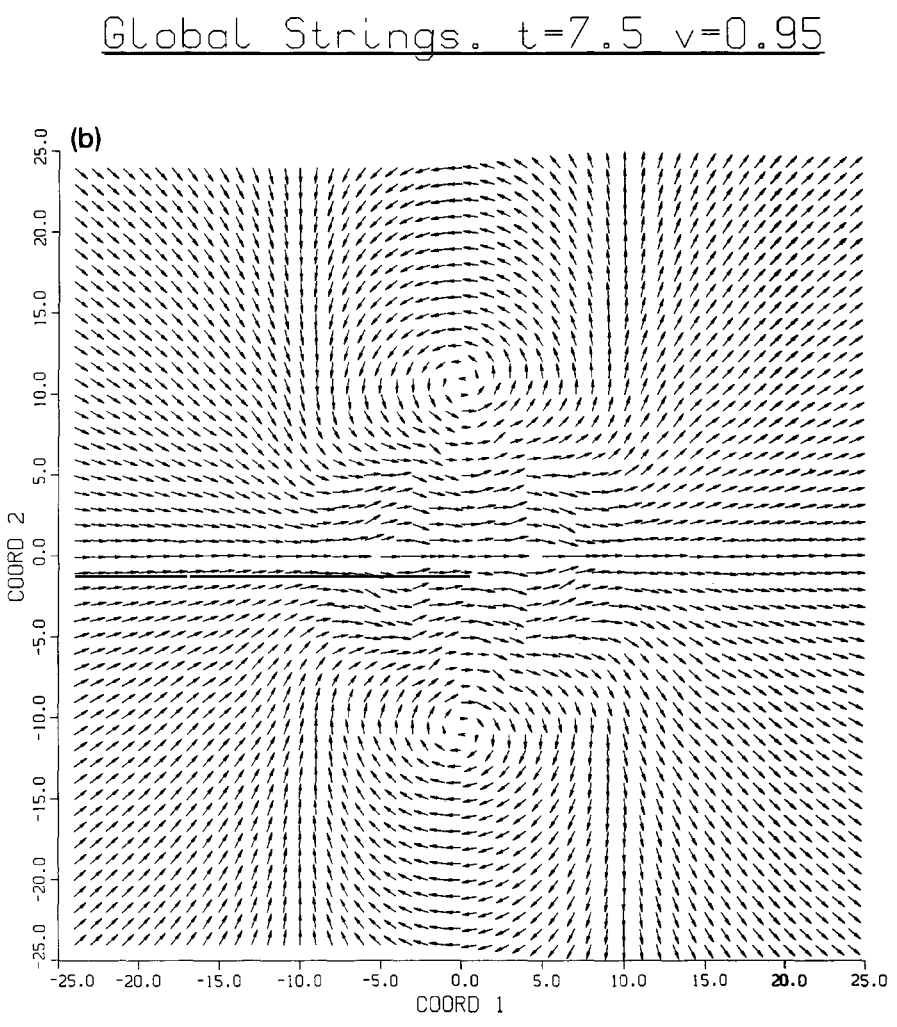


Fig. 10b.

The velocity effects on the interactions were studied by boosting the vortex configurations. In the vortex–vortex system, scattering through 90° was observed for scattering velocities larger than 0.9 with respect to the center of mass (fig. 10). For smaller velocities no scattering occurred due to the repulsive interaction. Notice that the emerging scattered vortices are not identical to the original ones: the field phase is rotated by 90° in their vicinity. These vortices may be viewed as the evolved highly distorted field lines that were connecting the original two vortices. Pursuing this observation further may lead to a plausible analytical understanding of the right angle scattering of vortices which is in turn closely

related to the intercommuting of cosmic strings [11]. Such an investigation is currently in progress.

The vortex–antivortex system failed to annihilate when the collision velocities in the center of mass frame were larger than the critical value $v_c = 0.9$ (fig. 11). Notice however that as in the vortex–vortex case the field around the vortices that survived annihilation has acquired an additional phase which in this case is equal to $\pi$.

The above analysis for vortices was extended to the case of global monopoles. A pair of monopoles was considered at positions $\boldsymbol{r}_1$ and $\boldsymbol{r}_2$ along the $z$-axis at $\pm z_0$.

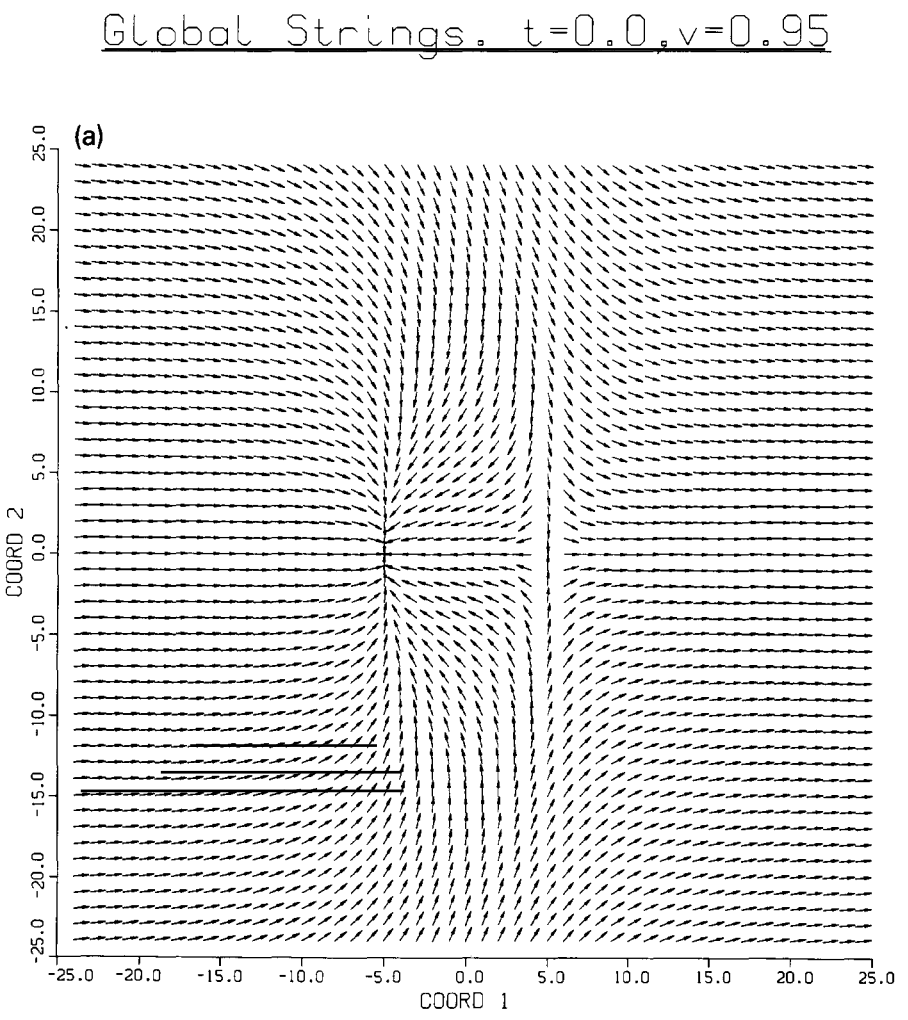


Fig. 11. Vortex–antivortex scattering above the critical velocity $v_c = 0.9c$. The initial velocity was $0.95c$. (a) $t = 0$, $v = 0.95c$; (b) $t = 7.5$. Notice the additional phase equal to $\pi$ acquired by the emerging vortices.

The two-vortex ansatz may be easily generalized in the case of monopoles as

$$\Phi_1 = \sin(\theta_1 \pm \theta_2)\cos\varphi,$$

$$\Phi_2 = \sin(\theta_1 \pm \theta_2)\sin\varphi,$$

$$\Phi_3 = \cos(\theta_1 \pm \theta_2). \tag{4.6}$$

Notice that both signs in this case refer to monopole–antimonopole pairs (this is easily seen by calculating the topological charge around each pole). In spite of this, it will be seen that the interaction is repulsive (attractive) for the plus (minus) sign.

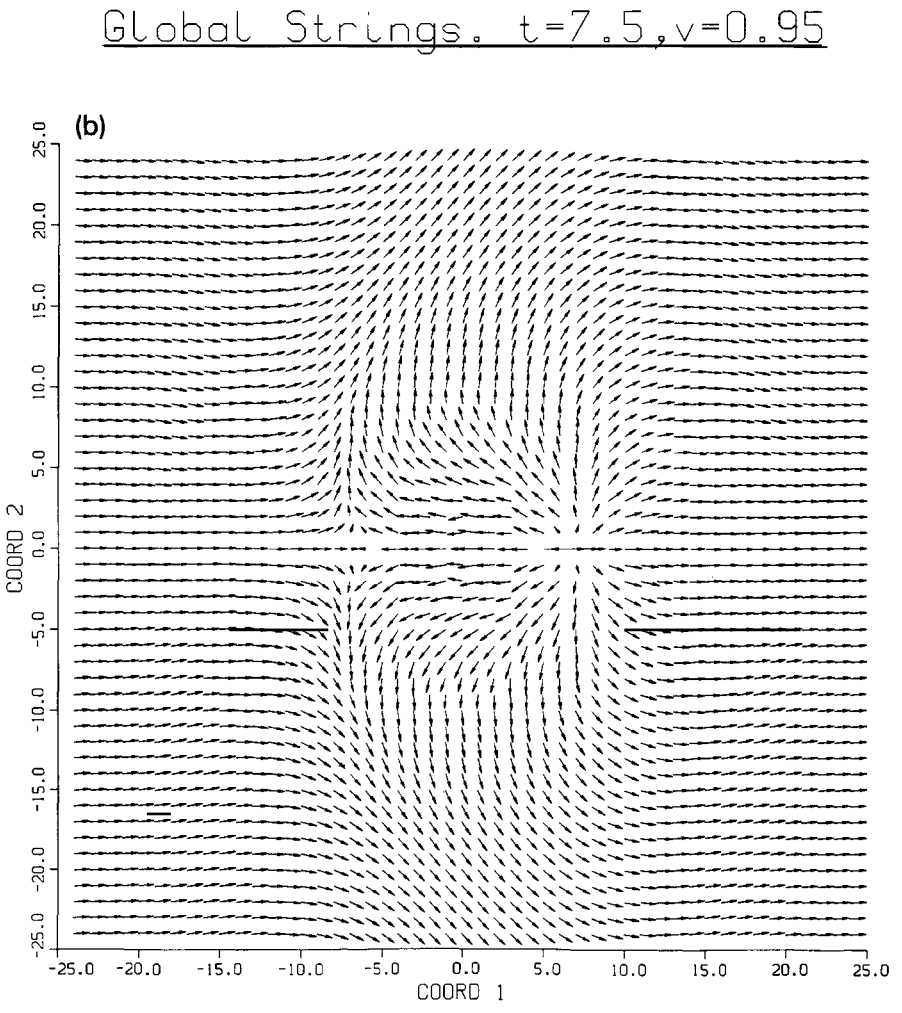


Fig. 11b.

Thus strictly speaking the statement that "monopoles–antimonopoles always attract" is incorrect.

Using the same method as for the case of vortices we may obtain the interaction energy density for each configuration. The result is

$$\varepsilon_{\text{int}}^{+} = \frac{2(z^2-a^2)}{(r^2+a^2)^2},$$

$$\varepsilon_{\text{int}}^{-} = -\frac{2(r^2-a^2)}{(r^2+a^2)^2}. \tag{4.7}$$

The interaction potential obtained by integration is

$$E_{\text{int}}^{+} = 2\int_L \mathrm{d}^3 r \frac{z^2-a^2}{(r^2+a^2)^2} = -8\pi a \tan^{-1}\left(\frac{L}{a}\right) + 4\pi L \frac{(L^2+3a^2)}{3(L^2+a^2)}$$

$$\simeq -4\pi^2 a + \frac{4\pi L}{3},$$

$$E_{\text{int}}^{-} = -2\int_L \mathrm{d}^3 r \frac{r^2-a^2}{(r^2+a^2)^2} = 16\pi a \tan^{-1}\left(\frac{L}{a}\right) - 8\pi L \frac{L^2-2a^2}{L^2+a^2} \simeq 8\pi^2 a - 8\pi L, \tag{4.8}$$

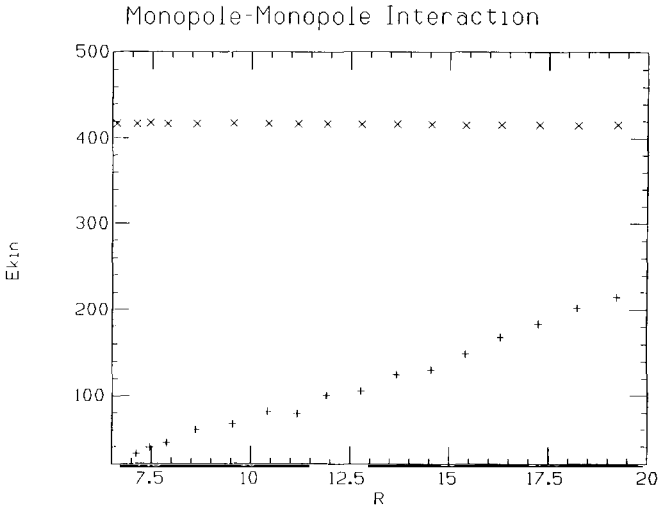


Fig. 12. The kinetic energy of a repelling monopole–antimonopole configuration as a function of the monopole distance $R$ (+ symbol). The functional relation is linear to a good approximation. The slope is $17 \pm 3$ consistent with the predicted value $2\pi^2$. The conserved total energy is also plotted ($\times$ symbol).

with $L \gg a = R/2 \gg 1$ where $R$ is the monopole–antimonopole distance and $L$ is the imposed cutoff. The corresponding force is

$$F_{\text{int}}^{+} = 8\pi \tan^{-1}\left(\frac{L}{a}\right) - 8\pi \frac{aL(7L^2 + 3a^2)}{3(L^2 + a^2)^2} \simeq 4\pi^2,$$

$$F_{\text{int}}^{-} = -16\pi \tan^{-1}\left(\frac{L}{a}\right) + 16\pi \frac{aL(2L^2 + a^2)}{(L^2 + a^2)^2} \simeq -8\pi^2. \tag{4.9}$$

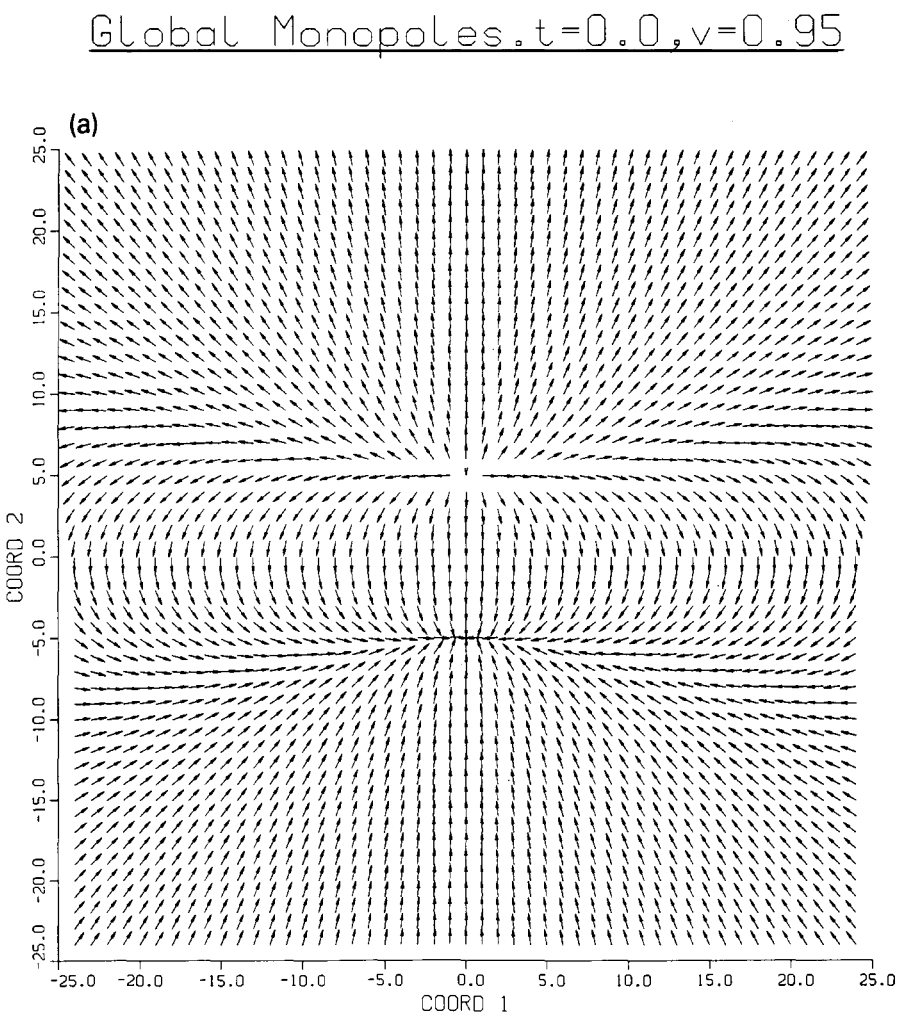


Fig. 13. Scattering of a repelling monopole–antimonopole pair. The initial velocities in the center of mass frame were $0.95c$. (a) $t = 0$, $v = 0.95c$; (b) $t = 7.5$. An expanding ring of vorticity emerges after the scattering. Its projection on the $x-z$-plane is shown in fig. 13b.

We have verified the above interaction potential for monopoles by evolving the initial configuration (4.6). The code described in sect. 2 was used with the appropriate initial conditions. As predicted, the interaction for the configuration with the plus (minus) sign was repulsive (attractive). Fig. 6 demonstrates the attraction and annihilation of a "minus" type monopole–antimonopole pair. In fig. 12 we plot the field kinetic energy $E_{\text{kin}}$ versus the monopole separation $R$ for the repulsive case. The slope predicted by the derived interaction potential is $2\pi^2$. The slope obtained by the simulation is $17 \pm 3$ consistent with the analytical prediction.

Boosted configurations were also studied in the monopole case. Initial velocities $v_i = 0.95$ were sufficient to overcome the repulsive interaction and lead to scatter-

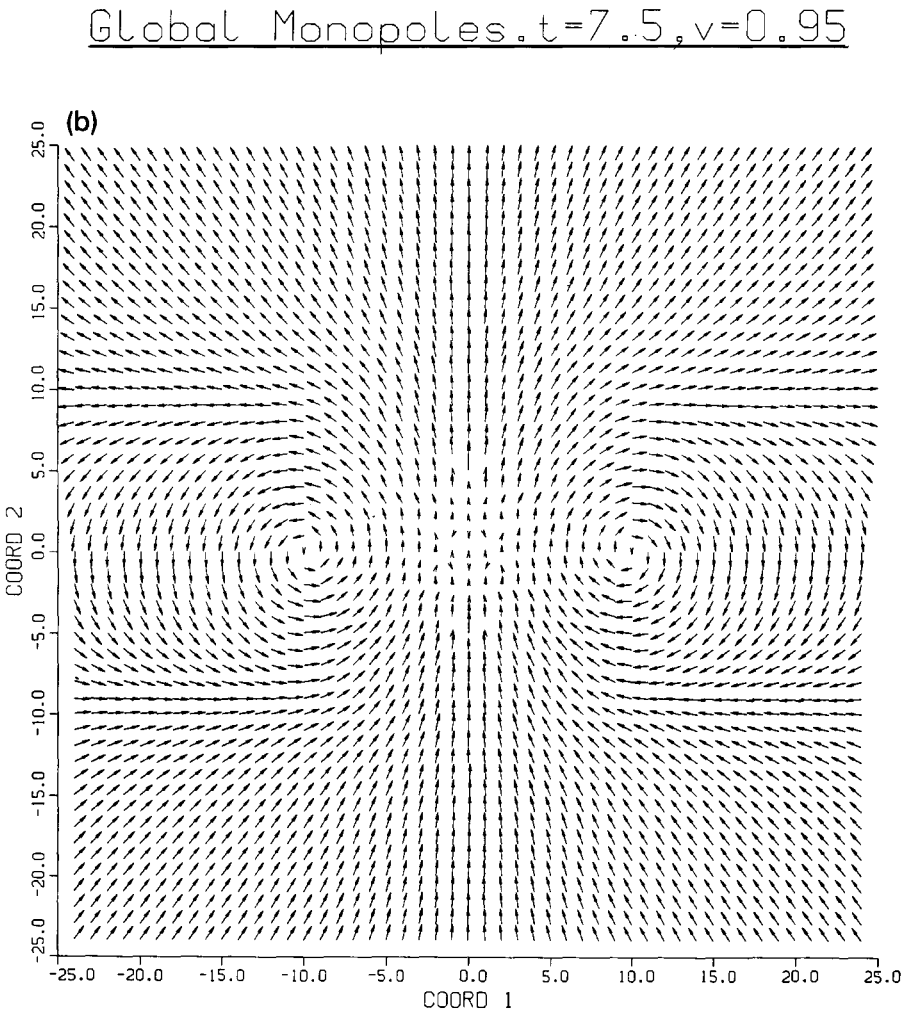


Fig. 13b.

ing. The finite size of the lattice may become a problem in simulating the scattering of highly Lorentz contracted defects. In particular scattering velocities larger than a threshold that depends on the lattice spacing may lead to disintegration of the scattering defects [3] followed by violation of energy conservation. No such problems were present for the scattering velocities considered here. The emerging configuration after the scattering was a ring shaped vortex expanding at right angles with respect to the line of incidence. The projection of this configuration on the $x$–$z$-plane is shown in fig. 13. This is consistent with the corresponding result for vortices where the scattered defects could be viewed as remnants of the

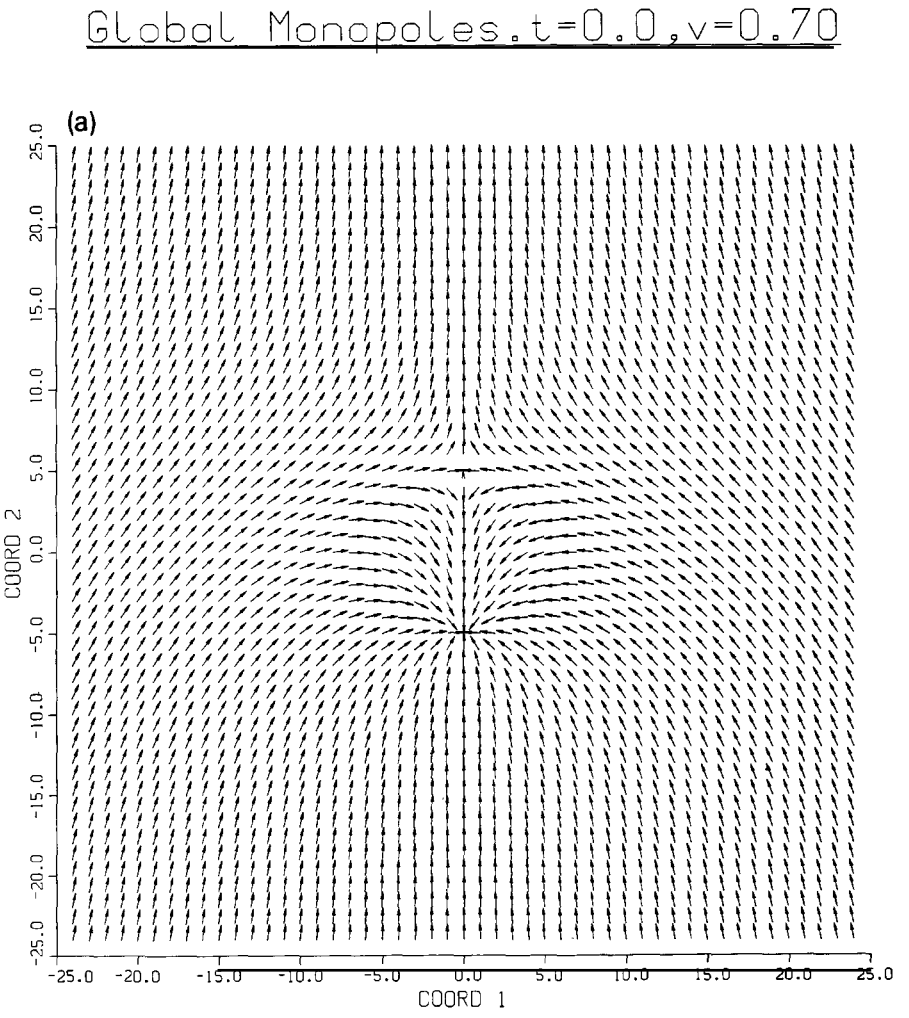


Fig. 14. Scattering of attracting monopole–antimonopole pair with velocities above the critical $v_c = 0.8c$. The initial velocity was $0.7c$. (a) $t = 0$, $v = 0.7c$; (b) $t = 7.5$. The emerging configurations are reflected as in the case of vortices.

field lines connecting the two incident vortices. By boosting an attractive monopole–antimonopole configuration we determined the critical velocity $v_c$ above which the monopoles failed to annihilate and went through each other (fig. 14). The obtained critical velocity is $v_c = 0.8$, slightly less than the one for vortices. This difference is probably due to the stronger interactions between monopoles which rapidly accelerate them at small distances.

At present there is no detailed analytical understanding for the existence of the above described critical velocities. An investigation in this direction is currently in progress.

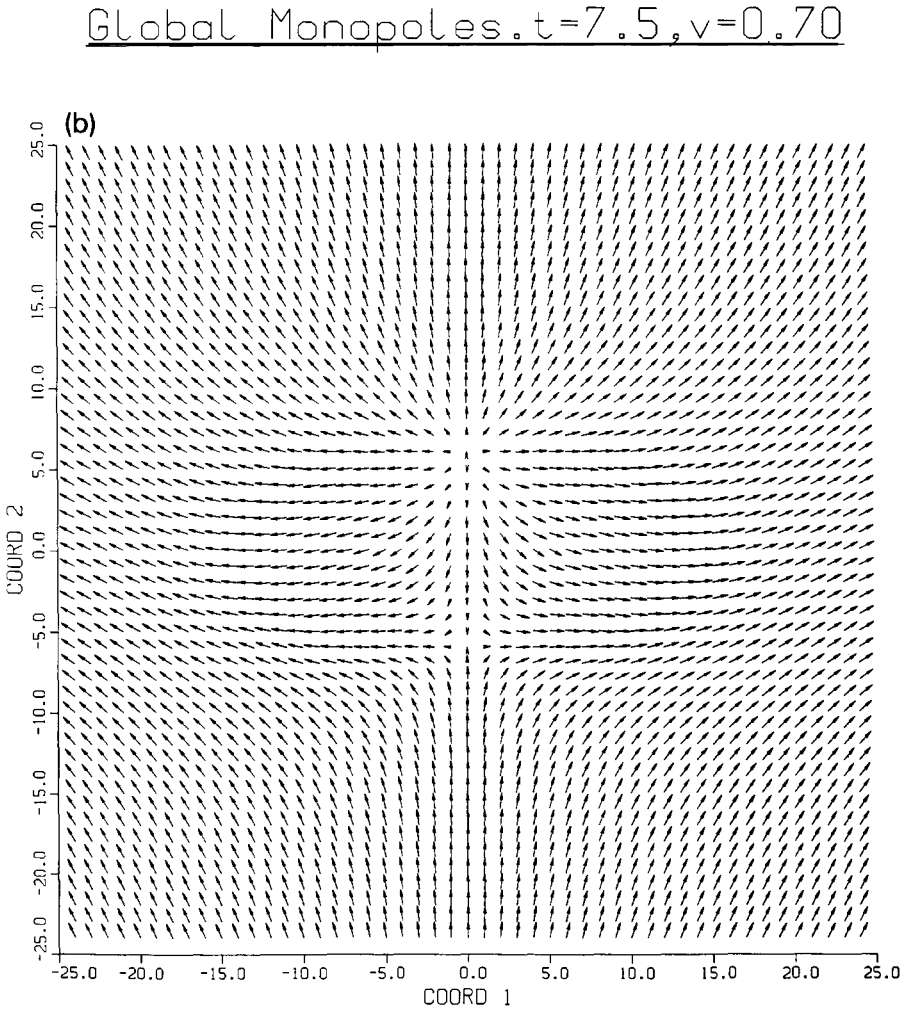


Fig. 14b.

## 5. Conclusions

A wide range study of the dynamics of vortices and global monopoles has been performed. Our results have several implications for both the cosmological effects and the field theoretical properties of the above topological defects.

The radial stability of both vortices and global monopoles has been verified by showing that the hamiltonian has a minimum with respect to a radial rescaling parameter $\alpha$. This minimum is a manifestation of the balance between the angular gradient energy and the potential energy of the defects. It leads them to oscillate radially after their formation until (and if) they stabilize by dissipation. Such oscillations were indeed seen in our simulations but are expected to rapidly damp out in an expanding background.

The virial theorems obtained as the conditions for minimizing the defect energy, provide analytical information for the non-asymptotic behavior of the vortex and global monopole fields. Generalizing this method may lead to obtaining higher moments of the defect fields by introducing parameters and minimizing with respect to them.

Even though we have shown that the instability of ref. [2] will not be realized in realistic situations where the monopole cores are free to move, it may have some consequences of academic interest. For example a perturbed monopole whose core has been artificially fixed (e.g. by boundary conditions or by interactions with a background) may indeed go through the unwinding described in ref. [2]. Such cases have been reported in refs. [5] and [9].

The derivation of the interaction potential for the global defects studied in this paper may be used to investigate the statistical mechanics of these defects. Such analytical calculations could be important especially in cases where large scale numerical simulations are impossible as in the case of vortices in three dimensions.

Our numerical simulations demonstrating the interactions of global defects have led to several interesting results. First, it was shown that the right-angle scattering of vortices is not strictly speaking a scattering process. The field around the emerging vortices has an additional phase equal to $\pi/2$ compared to the phase of the incident ones. This additional phase is easily understood if the scattering process is viewed as an evolution of the field lines. The emerging vortices are the evolved field lines that were connecting the original vortices (fig. 10). This argument extended to the case of global monopoles would predict an expanding ring of vorticity forming after the scattering. This ring is indeed seen in our simulations (fig. 13).

Topological defects with attractive interactions and relative velocities larger than a critical value $v_c$ failed to annihilate in our simulations. The critical velocity measured just before the cores started overlapping was $0.9c$ for vortices and $0.8c$ for global monopoles. The difference was attributed to the stronger interactions of global monopoles. The long-range interactions of global defects are expected to

introduce highly relativistic velocities during their evolution. Therefore the effects of the critical velocities should be carefully considered in any numerical or analytical study of global defect evolution. In particular the global monopole lifetime before annihilation takes place may increase significantly if the effects of critical velocities are considered.

The form of the derived interaction potential and the results of the simulations have shown that it is not the topological charge that determines the type of interaction between global monopoles. In particular defects of opposite charge may either attract or repel depending on the field configuration. For example, defining a configuration $(\Phi_1, \Phi_2, \Phi_3)$ as a monopole (i.e. having positive topological charge), we have two distinct types of antimonopoles (i.e. having negative topological charge): (a) $(\Phi_1, \Phi_2, -\Phi_3)$ where only one of the field components has been reflected and (b) $(-\Phi_1, -\Phi_2, -\Phi_3)$ where all components have been reflected. As we have shown analytically and numerically, the former antimonopole configuration is attracted to the monopole while the later is repelled. Therefore the critical factor that determines the topological defect interactions is not their topological charge; it is the relative phase of their field configurations. A detailed study of the effects of the relative phases of topological defects is in progress.

I would like to thank Robert Leese and Robert Brandenberger for stimulating comments and discussions. This work was supported by the US DOE under grant DE-AC02-76ER03130 Tasks K & A.

## References

[1] A. Vilenkin, Phys. Rep. 121 (1985) 263
[2] A.S. Goldhaber, Phys. Rev. Lett. 63 (1989) 2158
[3] E.P.S. Shellard, Nucl. Phys. B283 (1987) 624
[4] S.H. Rhie and D.P. Bennett, Phys. Rev. Lett. 65 (1990) 1709
[5] A. Pangellis, N. Turok and B. Yurke, preprint PUPT-91-1248 (1991)
[6] N. Turok, Phys. Rev. Lett. 63 (1989) 2625
[7] D. Harari and C. Loustó, Phys. Rev. D 42 (1990) 2626
[8] M. Barriola and A. Vilenkin, Phys. Rev. Lett. 63 (1989) 341
[9] D.P. Bennett and S.H. Rhie, Phys. Rev. Lett. 65 (1990) 1709
[10] E. Muller-Hartmann, Phys. Lett. 23 (1966) 521
[11] E.P.S. Shellard and P.J. Ruback, Phys. Lett. B209 (1988) 262
[12] L. Perivolaropoulos, Large scale structure with global monopoles and cold dark matter, Mod. Phys. Lett. A, to appear